Biointerface Research in Applied Chemistry
Open-Access Journal (ISSN: 2069-5837)

Article
Volume 13, Issue 2, 2023, 118
https://doi.org/10.33263/BRIAC132.118

Investigation of Structural and Mechanical Properties of Nanostructured TiMgSr Alloy for Biomedical applications

Pradeep Navilehal Basavarajappa [1,*], Muduvalli Mahabala Rajath Hegde [1], Shashanka Rajendrachari [2,*], Attukalathil Orongil Surendranathan [3]

[1] Department of Mechanical Engineering, JNN College of Engineering, Shivamogga, Affiliated to Visvesvaraya Technological University, Belagavi, 590018, India; pradeepnb@jnnce.ac.in (N.B.P); Orcid id: 0000-0001-5041-8331; rajathhegdemm63@jnnce.ac.in (M.M.R); Orcid id: 0000-0003-1456-9751
[2] Department of Metallurgical and Materials Engineering, Bartin University, Bartin, Turkey; shashankaic@gmail.com (S.R.); Orcid id: 0000-0002-6705-763X
[3] Department of Metallurgical and Materials Engineering, National Institute of Technology Karnataka, Surathkal-575025, Mangalore, Karnataka, India; nathan@nitk.ac.in (A.O.S.); Orcid id: 0000-0002-7715-2008
* Correspondence: pradeepnb@jnnce.ac.in (N.B.P.); shashankaic@gmail.com (S.R);

Scopus Author ID 55851104900
Received: 13.12.2021; Accepted: 10.01.20222; Published: 24.03.2022

Abstract: In this study, Nanostructured TiMgSr alloy is produced by cold Isostatic Pressing (CIP) followed by microwave sintering. The fabricated alloy results in the formation of solid binary solutions along with the elemental phases. The CIP compacted alloy was characterized using X-ray diffraction (XRD) and scanning electron microscopy (SEM) to investigate the phases and the morphology. The presence of intermetallic phases $SrTiO_3$ and $Mg_{17}Sr_2$ along with elemental Ti, Mg, and Sr crystallites with a narrow peak during the sintering process is prevalent; however, the crystallite size was retained in the nanoscale regime around 58 nm. The developed titanium alloy exhibits a low Young's modulus and good strength. The young's modulus of Ti–Mg–Sr alloys was around 48.11 GPa, significantly closer to human cortical bone (10–30 GPa). Among so far developed Ti-based alloys, the CIP consolidated Ti-Mg-Sr alloy results in low young modulus and hardness. In the future, it may be used practically for biomedical applications.

Keywords: XRD; nanohardness; cold isostatic pressing (CIP); Young's modulus; TiMgSr alloys.

1. Introduction

The transition of materials from the macroscale to the nanoscale can cause significant physical and chemical properties [1-5]. Physical properties between bulk and nanoscale materials are driven by quantum confinement phenomena and/or the increasing prevalence of surface atoms [6]. Topological alterations at the nanoscale can result in significant changes in physical attributes [7-9]. Hence, developing dependable procedures to produce nanomaterials in assorted sizes and chemical compositions is a hot topic in nanotechnology research [10]. Traditional metal sol synthesis methods, which have been around since Michael Faraday's time, are still used to make metal nanoparticles; there have been several improvements and modifications to the methods that allow for more control over the shape, size, and other properties of nanograins. These advancements have allowed researchers to investigate quantum confinement and other features that are affected by size, shape, and composition. Though nanoparticle synthesis and organization are useful tools for nanotechnology, converting

nanoparticles or nanopowders into bulk shapes while keeping their nanosize is challenging in biomedical applications [11, 12].

At present, titanium-based alloys are finding more attention in developing metallic biomaterials because of their outstanding specific strength and corrosion resistance, no allergic problems, and the best biocompatible nature among metallic biomaterials [13]. The addition of Mg to Ti results in the production of alloys with low-density and high specific strength [14, 15]. Many investigations have shown that the introduction of Mg to Ti results in producing alloys of low-density and high specific strength, which reduces density by about 3 to 5 times as much as it raises strength and modulus, thereby resulting in the fall of the structural weight of alloy materials. The introduction of Sr into Mg is desirable as one of the excellent future constituents in the development of Ti alloys to improve biological and mechanical performance. [16-19]. Table 1 presents recent investigations into titanium-based metallic materials in biomedical applications.

Table 1. Summary of recent research on Ti-based alloys for biomedical applications.

Alloys	Views	References
TiN	The results show that laser-synthesized TiN NPs are safe for biological systems, leading to new phototheranostic modalities.	[20]
TiMg composite	Developed low modulus Ti/Mg interpenetrating phase composite results in Young's modulus like that of human bone, suitable for biological uses.	[21]
$Ti_{13}Nb_{13}Zr$	The surface hardness of Ti13Nb13Zr increases with increasing ZnO percentage in HA due to plasma-sprayed HA-ZnO coatings.	[22]
TiO_2 microfibers with PHO	Studies on polyhydroxy octanoate-based composites containing TiO2 microfibers support cell survival and migration.	[23]
Ti-Mo	Ti-Mo alloys, the trend in overall hardness found identical for relative density resulting in Ti-16 wt.% Mo as hardest alloy material.	[24]
Zn–3Cu and Zn–3Cu–0.2Ti	Investigation shows the highest wear resistance of AC Zn–3Cu–0.2Ti.	[25]
Ti–Nb	The addition of alloying elements has improved the superelasticity of the alloy.	[26]
Ti-Mo–B_4C	Achieved good mechanical properties for the Spark plasma sintered composites at elevated temperatures.	[27]
Ti-20Zr-Mo	Results showed an increase in hardness and reduction in elastic modulus as the Mo content increases.	[28]
Ti-Zr	The study reveals that, as the Nb content increases, the Ti-Zr alloy shows good biomechanical properties.	[29]

Transformation of nanostructured/amorphous/supersaturated solid solution powder into a solid bulk form is a challenging task due to grain development, recrystallization, and the production of ordered structures from nonequilibrium phases. Studies of alloy powder consolidation by warm pressing, SPS, hot pressing, explosive compaction, and warm extrusion have been published [30, 31]. In the isostatic pressing process, a uniform pressure is exerted on all the powder's external surfaces simultaneously. As no lubricant is needed, the powder is compacted to the same pressure across all directions, resulting in a highly uniform density. The powder is enclosed in a flexible mold and then dipped in a fluid kept at an extremely high pressure to achieve uniform pressure across the powder particles. The factors that affect the geometry of parts compacted unidirectionally in rigid dies are removed by isostatic pressing. Cold isostatic pressing refers to isostatic pressing at room temperature (CIP). The CIP is primarily used to create green bodies (powder compacts before sintering). It is possible to achieve pressures of up to 700 MPa using the CIP process [32]. Compared to other pressing processes, CIP results in a more uniform pressure distribution. Compaction characteristics are improved by removing air from powder particles before compaction. In the CIP process,

lubricant reduction prior to sintering is eliminated [33]. On the other hand, mechanically alloyed TiMgSr powder was not cemented by CIP compaction followed by microwave sintering. Hence, the present investigation is on synthesizing bulk nanostructured TiMgSr alloys by cold isostatic pressing followed by microwave sintering for biomedical applications. The compact sample prepared by CIP is examined for structural and mechanical properties by XRD, SEM, and nanoindentation. Further, the nano hardness along with the elastic modulus of sintered pellets was determined by a load-displacement curve using the Berkovich indenter of a three-sided pyramid with midline and three faces [34].

2. Materials and Methods

Ti, Mg, and Sr of purity 99.99 % in atomic percent 70:10:20 are mechanically alloyed by ball milling using Retsch PM-100 ball equipment. Milling was conducted at a speed of 200rpm in a ratio of 10:1 (ball to powder weight ratio) with tungsten carbide (WC) as the milling media for 30 hours.

CIP was used to consolidate ball-milled powders by applying pressure to the powder using a liquid medium of glycol mixed with water. The powder is placed in a flexible mold. Typically, a pressure of 300 Mpa is exerted to compress and produce a solid compact of a high density capable of undergoing sintering.

The structural properties of CIP consolidated microwave sintered bulk samples were examined by an X-ray diffractometer (XRD) with Cu radiation (0.1542 nm). Using Bragg's and Scherrer's equations, structural characteristics such as lattice parameters (abc) and average crystallite size (D) are determined. The Scherrer formula was used to compute crystallite size (D), and Xpert high score plus software was used for profile fitting [35–37].

Further, the microstructure of the sintered compacted samples was examined by JEOL SEM IT 300 with a 30 kV Tungsten source SEM for imaging. Thus, XRD and SEM were used to determine the structure of the compacted samples.

The nanoindentation test examined the mechanical characteristics of the sintered compacted sample by measuring the values of Young's modulus and nano hardness of the compacted sample from a load-displacement curve using a Berkovich type of indenter [38].

3. Results and Discussion

The results of XRD, SEM, and nanoindentation characterization of sintered compacted CIP samples are discussed.

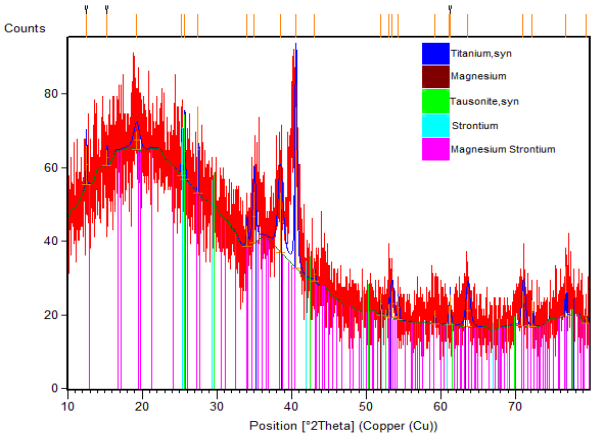

Figure 1. XRD Profile of Sintered Compacted sample.

Table 2. XRD results of Sintered compacted sample.

Position (2θ^0)	Structure	Compound name	Crystallite size 'D' nm
25.35	Cubic	Strontium	58.2nm
25.42	Cubic	Tausonite, syn	
63.58	Hexagonal	Magnesium	
76.82	Hexagonal	Titanium	
29.45	Hexagonal	Magnesium Strontium	

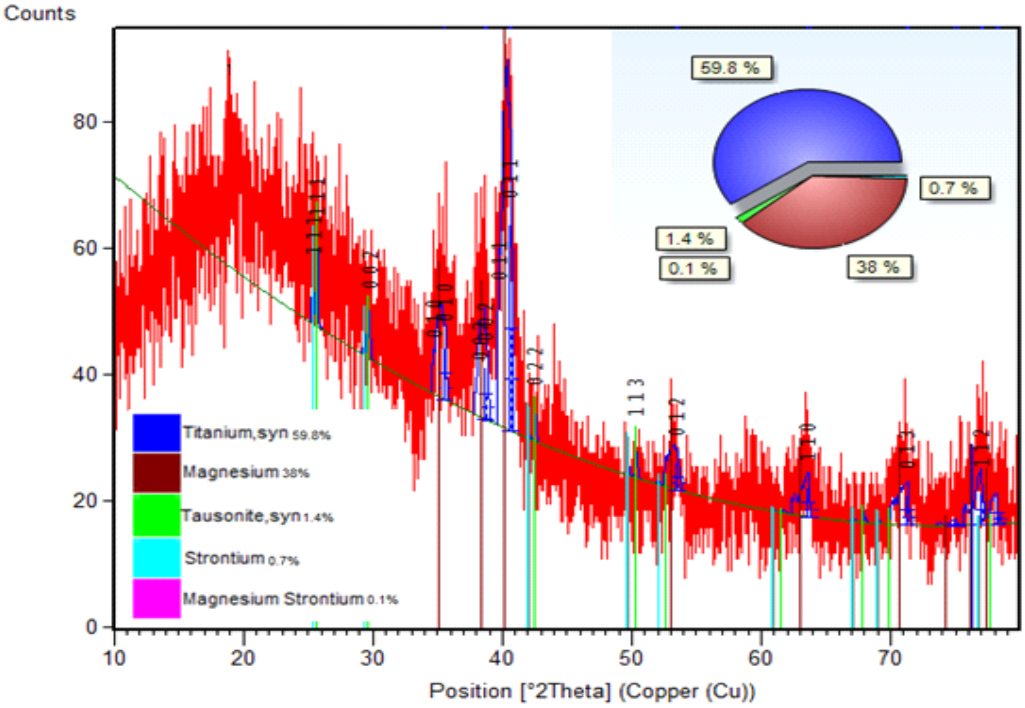

Figure 2. Rietveld analysis of Sintered Compacted sample.

Table 3. Structural parameters of Sintered compacted sample.

Position (2θ)	Height [counts]	d-spacing [Å]	FWHM [2θ]	Lattice parameters in nm	Miller indices/Phase	Phase percentage
25.35	8	3.518	0.1000	6.1240	111/Sr	0.7
25.42	6.37	3.521	0.1574	6.0460	111/SrTiO3	1.4
63.58	8.03	1.463	0.6298	a=b=3.2194, c=5.2009	110/Mg	38
76.82	1.11	1.239	0.9600	a=b=2.9496, c=4.6762	112/Ti	59.8
29.45	24.24	3.248	0.2590	a=b=10.5296 c=10.3568	002/Mg17Sr2	0.1

XRD results of the consolidated sample indicate narrowing and smoothening of Bragg peaks with high intensities, as shown in Figure 1. These trends show a transition from amorphous to crystalline structure because of the mechanical alloying of powder for 30 hours. The XRD pattern shows Ti, Mg, and Sr elemental peaks along with the presence of intermetallic peaks, SrTiO3 and Mg17Sr2. The XRD profile presents a narrow peak (peak 2 = 40.5700, FWHM = 0.3149, height = 28.5). The significance of peak narrowing is due to an increase in crystallite size (58.2nm) as compared to the 30hr mechanically alloyed powder (32.07nm) as reported in the literature [39]. The presence of more than one intermetallic phase with peak narrowing suggests that conversion from a partially disordered structure to almost complete ordering during the consolidation process. During the mechanical alloying process with high energetic ball milling, powder particles experience SPD (severe plastic deformation), due to which materials undergo disordered structures to varying degrees [40-45]. In the recent

investigation, an almost complete state of disorder was noticed at 30 hrs of ball milling duration [39]. Such a state is a phenomenon of changes in the material structure because of CIP processing at elevated temperatures. Retaining nanocrystalline and amorphous phases is a difficult challenge during the consolidation process. Such a phenomenon is shown by the presence of similar phases in the present investigation, as shown in XRD results in Table 2.

Furthermore, the indexing and quantification of each phase are analyzed by Rietveld fitment of the XRD profile using high score software. Figure 2 depicts the Rietveld analysis of the sintered sample. The analysis observed that the formation of intermetallic compounds is identical with previous results of 30hr ball milled powder [39]. However, among the intermetallic phases, the presence of $Mg_{17}Sr_2$ is very minute it may be due to the metallurgical changes that occur during the sintering process.

3.2. Scanning electron microscope (SEM) characterization of the sintered compacted sample.

Figure 3 reveals the FESEM images of the CIP consolidated compacts obtained from 30 hrs of MA powder. The current consolidation technique produced a void-free microstructure. Since the CIP consolidation process is a low temperature (200°C) synthesis method, porosities are observed. Diffusion bonding is not immense; hence porosities are bound to remain. In addition, strain-hardened ball milled powder requires high compaction pressure during consolidation. Agglomeration of nanoparticles is observed because of compaction. It is hereby noted that consolidation by the CIP method can retain nanocrystalline grains in the consolidated sample, as observed from the micrographs [46].

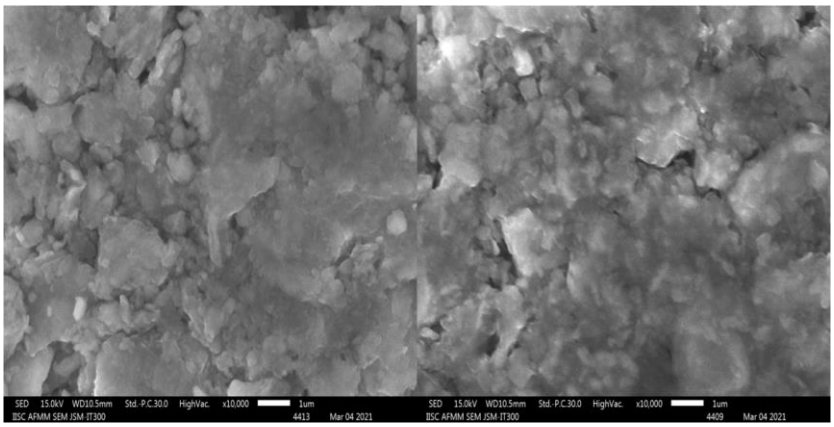

Figure 3. Micrograph of the sintered compacted sample.

3.3. Nanoindentation test of a sintered compacted sample.

Nanoindentation test was used to determine the mechanical properties like nanohardness and elastic modulus of the sintered TiMgSr on 30hrs of mechanically alloyed CIP compacts by Berkovich, Diamond indenter. The Berkovich indentation print and the surface state are represented in Figure 4.

The test was carried out on three trails with three locations on the sample were performed. The load-displacement curve of each trail performed on 3 different locations is represented in Figure 5. Load and displacement are measured as the tip of the indenter progress into the sample's surface by the predefined profile of loading and unloading during a test. Pop in the phenomenon is not observed in the load-displacement curves. Such a phenomenon is because of large-scale dislocation motion with the onset of plastic deformation and a pore or

vacancies existing in the crystal structure below the advancing indenter [47]. The load required to penetrate 600nm to 1300nm of depth was found to be 28mN for locations 1 to 3.

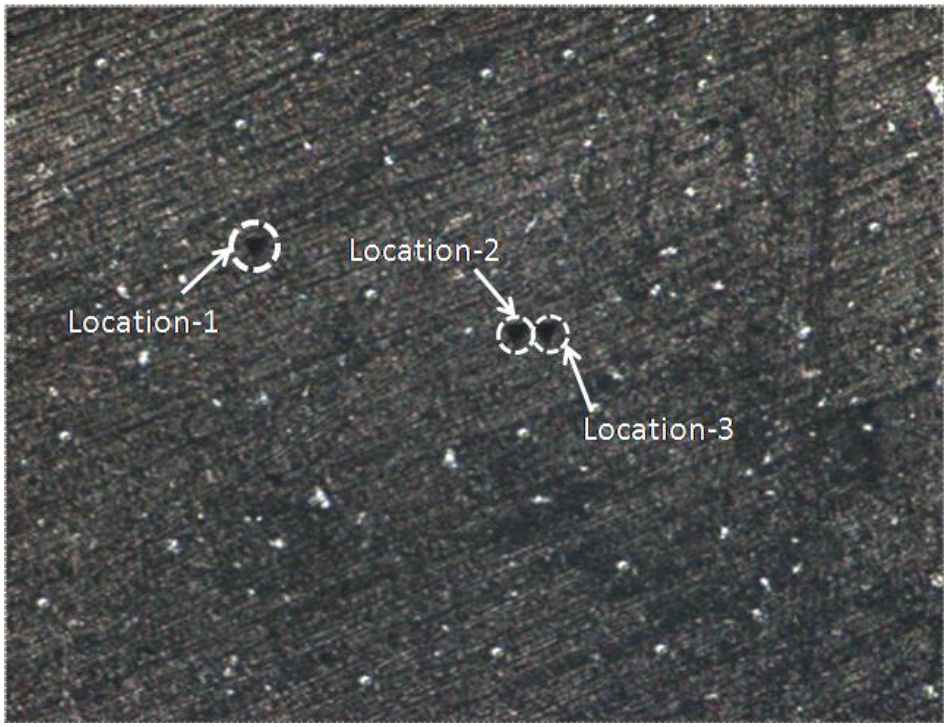

Figure 4. A picture representing indentation performed on CIP compact.

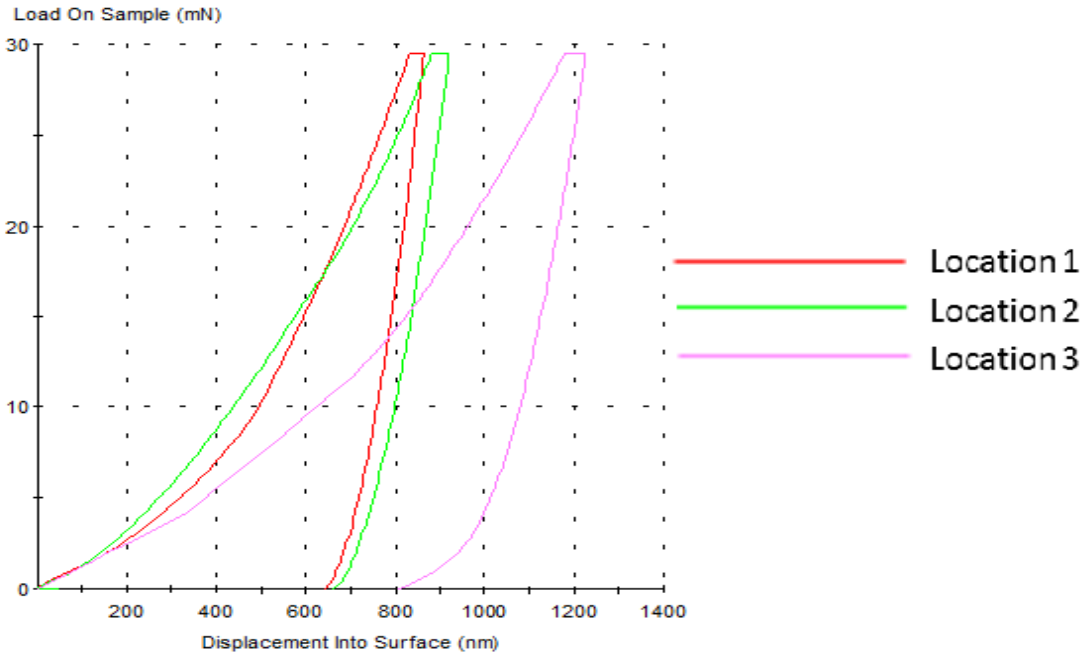

Figure 5. Load- displacement curve of 30hrs mechanically alloyed compact(CIP) sample.

Figure 6 (a) depicts the hardness curve of mechanically alloyed CIP compacts after 30 hours for locations 1 to 3. It is observed that the hardness value varies from 2.2 GPa to 3 GPa, wherein the average hardness is found to be 3.072 Gpa. During the displacement of the indenter from 800 to 1300 nm, the hardness was found to be decreasing.

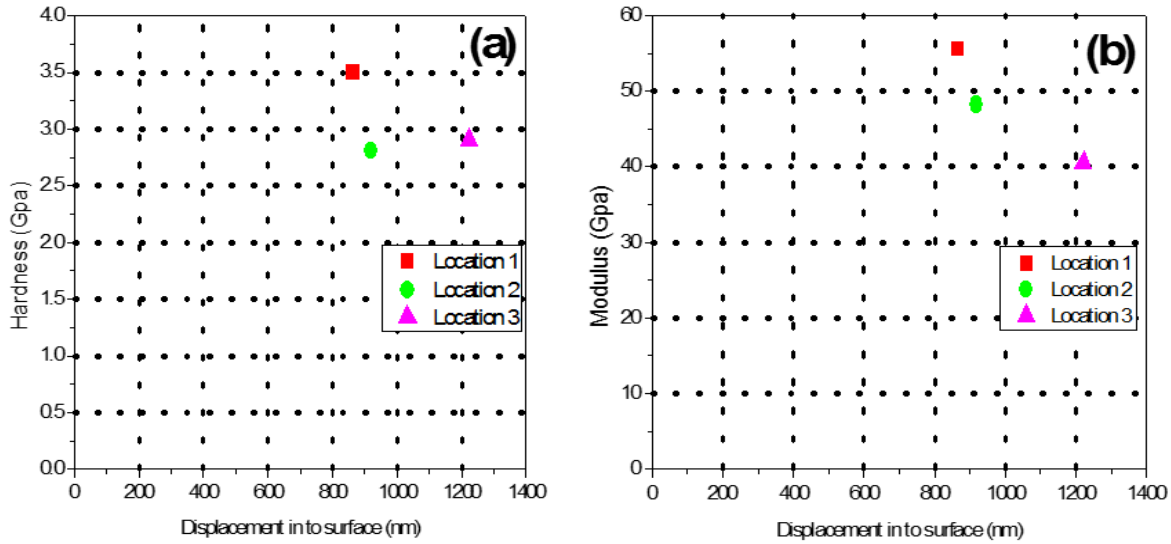

Figure 6. (**a**) Hardness and (**b**) Elastic modulus curve of 30hrs mechanically alloyed compact(CIP) sample.

Using the below Berkovich equation, loading charge divided by the exposed contact area Ac, the hardness can be computed [32].

$$H = \frac{P_{max}}{A_c} \quad (1)$$

where the maximum applied load is P_{max}, and the contact area is A_c.

Nano-indentation is a technique for evaluating the elastic and plastic characteristics of materials at the nanoscale level in a single experiment that does not require extra sample preparation (however, a good surface finish is needed). In nanoindentation, the indentation process's force, displacement, and time are all continually measured. Er stands for reduced elastic modulus.

$$E_r = \frac{\sqrt{\pi}}{2C}\frac{1}{\sqrt{A_c}} \quad (2)$$

where A_c and C stand for the projected contact area and the indenter-to-sample contact compliance, respectively.

$$C = C_t - C_f = \frac{dh}{dF} \quad (3)$$

where C_t, C_f, F, and h denotes the total compliance, frame compliance, force, and displacement.

$$\frac{1}{E_r} = \frac{1-\vartheta_s{}^2}{E_s} + \frac{1-\vartheta_i{}^2}{E_i} \quad (4)$$

where Poisson's ratios and elastic moduli of the sample and indenter are represented by ϑ_s, ϑ_i and E_s, E_i, respectively.

The Elastic modulus curve of 30hrs of mechanically alloyed CIP compacts for locations 1 to 3 as shown in Figure 6(b). Wherein the average elastic modulus is found to be 48.11 Gpa. During the displacement of the indenter from 600 to 1300nm of depth, the elastic modulus was decreasing.

Another problem with biomedical titanium alloys is their high modulus. Ti implants and prostheses have a high Young's modulus, preventing load transfer to the bones and providing a stress shield phenomenon. Because bone is a living substance, the stress-shielding

action causes a decrease in bone density, known as bone resorption [48]. Ti alloys with low modulus are undergoing extensive biomedical research. In this investigation, the average hardness and young's modulus of the sintered compacted alloy are presented in table 4. The hardness of the sintered sample was found to be higher, apart from the lowered Young's modulus, at 48.11 Gpa closer to the human cortical bone (10-30 Gpa) [49-51] and also lower than those of the commercially available CP-Ti biomaterial [52] (hardness of 2.55 GPa and young's modulus 107.33GPa respectively) and the most recent investigated Ti alloys as presented in Table 5.

Table 4. Measured values of Nanoindentation test.

	Average	**Maximum**	**Minimum**
Elastic modulus (GPa)	48.112	55.599	40.490
Hardness (GPa)	3.072	3.501	2.81

Table 5. Comparison of mechanical characteristics of various Ti-based alloys.

Alloy	**Elastic modulus (Gpa)**	**Hardness (Gpa)**	**Reference**
Ti–6Al–4V	109	4.09	[53]
Ti-48Al-2Nb-0.7Cr-0.3Si	166	-	[53]
Ti-24Nb-4Zr-7.9Sn	53	2.2	[53]
Ti-12Mo-5Zr-2Fe	74-85	-	[54]
Ti-10Mo-1.2Si-4Zr	23	-	[54]
Ti-10Mo-10Nb	24	-	[54]
Ti-12Mo	111	4.5	[24]
Ti-20Mo	127	4.8	[24]

4. Conclusions

The present investigation shows the importance of material characterization in the respective results of the various analyses performed. The main cause of peak narrowing indicates the increase in the crystallite size. Retaining the nanocrystalline and amorphous structures in the compacted sintered sample is a challenging task. However, in this investigation, mechanically alloyed powders with high-energy ball milling successfully retained nonequilibrium phases and structure.

The present work has shown increased crystallite size and indicates the importance of peak narrowing in XRD profiles of CIP consolidated compacts of mechanically alloyed powders. During the consolidation process, almost complete ordering of phases is observed. Such an ordering phase is indicated by the presence of more than one intermetallic phase and a reduction in peak broadening with high intensities. The measured values of the nanoindentation test show a low Young's modulus of 48Gpa and hardness of 3Gpa nearer to the human cortical bone compared to the so far developed βTi alloys. The morphological study observed that agglomeration of particles because of compaction and nano-sized particles are seen.

Funding

This research received no external funding.

Acknowledgments

The authors would like to acknowledge Dr. V B's ceramics research center, Chennai, and IISc Bangalore, for providing the compaction, XRD, and SEM facility.

Conflicts of Interest

The authors declare that they have no known competing financial interests or personal relationships that could have influenced the work reported in this paper.

Appendix: Details of ball milling

Ball milling specifications	
Ball to Powder weight ratio	10:1
Milling media	Toluene
Speed	200 rpm
Ball and Vial material	Tungsten carbide (WC)
Container (vial) volume	250 ml
Utility volume	50-150 ml
Diameter of ball	10 mm
Weight of each ball	7.5 gm

References

1. Shashanka, R. Synthesis of nanostructured stainless steel powder by mechanical alloying-an overview. *International Journal of Scientific & Engineering Research* **2017**, *8*, 588-594.
2. Shashanka, R. Effect of Sintering Temperature on the Pitting Corrosion of Ball Milled Duplex Stainless Steel by using Linear Sweep Voltammetry. *Anal Bioanal Electrochem* **2018**, *10*, 349-361.
3. Nayak, A.K.; Shashanka, R.; Chaira, D. Effect of NanosizeYittria and Tungsten Addition to Duplex Stainless Steel during High Energy Planetary Milling. *IOP Conf. Series: Materials Science and Engineering* **2016**, *115*, 1-7, https://doi.org/10.1088/1757-899X/115/1/012008.
4. Shashanka, R.; Chaira, D.; Swamy, B.E.K. Effect of Y_2O_3 nanoparticles on corrosion study of spark plasma sintered duplex and ferritic stainless steel samples by linear sweep voltammetric method. *Archives of Metallurgy and Materials* **2018**, *63*, 749-763, https://doi.org/ 10.24425/122401.
5. Shashanka, R. Non-lubricated dry sliding wear behavior of spark plasma sintered nanostructured stainless steel. *Journal of Materials and Environmental Sciences* **2019**, *10*, 767-777.
6. Magdalena, A. Smart Nanomaterials for Biomedical Applications-A Review. *Nanomaterials* **2021**, *11*, 1-33, https://doi.org/10.3390/nano11020396.
7. Shashanka, R.; Swamy, B.E.K. Simultaneous electro generation and electrodeposition of copper oxide nanoparticles on glassy carbon electrode and its sensor application. *SN Applied Sciences* **2020**, *2*, 956, https://doi.org/10.1007/s42452-020-2785-1.
8. Shashanka, R. Investigation of optical and thermal properties of CuO and ZnO nanoparticles prepared by Crocus Sativus (Saffron) flower extract. *Journal of the Iranian Chemical Society* **2021**, *18*, 415-427, https://doi.org/10.1007/s13738-020-02037-3.
9. Shashanka, R.; Jayaprakash, G.K.; Prakashaiah, B.G. Electrocatalytic determination of ascorbic acid using a green synthesised magnetite nanoflake modified carbon paste electrode by cyclic voltammetric method. *Materials Research Innovations* **2021**, https://doi.org/10.1080/14328917.2021.1945795.
10. Mostafa, Mabrouk.; Diganta, B. Das.; Zeinab, A. Salem. et al. Nanomaterials for Biomedical Applications: Production, Characterisations. Recent Trends and Difficulties. *Molecules* **2021**, *26*, 1077, https://doi.org/10.3390/molecules26041077.
11. Kolahalam, L.A.; Viswanath, I.K.; Diwakar, B.S.; et al. Review on nanomaterials: Synthesis and applications. *Materials Today: Proceedings* **2019**, *18*, 2182-2190, https://doi.org/10.1016/j.matpr.2019.07.371.
12. Ahn, B. Synthesis and Properties of Bulk Nanostructured Metallic Materials. *Metals* **2018**, *8*, 855, https://doi.org/10.3390/met8100855.
13. Antonio, F.; Antonio, R.; Joao, P.D. et al. Machining of titanium alloys for medical application - a review. *Proc IMechE Part B: J Engineering Manufacture* **2021**, 1–10, https://doi.org/10.1177%2F09544054211028531.
14. Sumit, B.; Satyam, S.; Kaushik, C. et al. Comprehensive review on alloy design, processing, and performance of β Titanium alloys as biomedical materials. *International materials reviews* **2021**, *66*, 114-139, https://doi.org/10.1080/09506608.2020.1735829.

15. Song, J.H.; Aqeel, A.; Raman, S. The effect of Mg content and milling time on the solid solubility and microstructure of Ti–Mg alloys processed by mechanical milling. *Journal of Materials Research and Technology* **2021**, *11*, 1424-1433, https://doi.org/10.1016/j.jmrt.2021.01.097.
16. Tejeda-Ochoa, A.; Kametani, N.; Carreño-Gallardo, C. et al. Formation of a metastable fcc phase and high Mg solubility in the Ti-Mg system by mechanical alloying. *Powder Technology* **2020**, *374*, 348-352, https://doi.org/10.1016/j.powtec.2020.07.053.
17. Rajesh, P.V. Titanium-based biomaterial for bone implants: A mini-review. *Materials Today: Proceedings* **2020**, *26*, 3148-3151, https://doi.org/10.1016/j.matpr.2020.02.649.
18. Puja, Y.; Kuldeep, K.S. Effect of heat-treatment on microstructure and mechanical properties of Ti alloys: An overview. *Materials Today: Proceedings* **2020**, *26*, 2546-2557, https://doi.org/10.1016/j.matpr.2020.02.541.
19. Na, X.; Jijiang, F.; Lingzhou, Z.; Paul, K. C.; Kaifu, H. Biofunctional Elements Incorporated Nano/Microstructured Coatings on Titanium Implants with Enhanced Osteogenic and Antibacterial Performance. *Adv. Healthcare Mater* **2020**, *9*, 1-20, https://doi.org/10.1002/adhm.202000681.
20. Zelepukin, I.V.; Popov, A.A.; Shipunova, V.O. et al. LasersynthesizedTiN nanoparticles for biomedical applications: evaluation of safety, biodistribution and pharmacokinetics. *Materials Science & Engineering C* **2021**, *120*, 1-39, https://doi.org/10.1016/j.msec.2020.111717.
21. Vladimirovich, OI.; Jana, W.; Soo-Hyun, J. et al. Anomalous compliance of interpenetrating-phase composite of Ti and Mg synthesized by liquid metal dealloying. *Scripta Materialia* **2021**, *194*, 1-5, https://doi.org/10.1016/j.scriptamat.2020.113660.
22. Puneet, B.; Gurpreet, S.; Hazoor, S.S. Improvement of surface properties and corrosion resistance of $Ti_{13}Nb_{13}Zr$ titanium alloy by plasma-sprayed HA/ZnO coatings for biomedical applications. *Materials Chemistry and Physics* **2021**, *257*, 123-738, https://doi.org/10.1016/j.matchemphys.2020.123738.
23. Ivana, M.; Ruggero, F.; Anjani, K.M. et al. Polyhydroxyoctanoate films reinforced with titanium dioxide microfibers for biomedical application. *Materials Letters* **2021**, *285*, 1-5, https://doi.org/10.1016/j.matlet.2020.129100.
24. Mehdi, S.A.; Seyed, A.D.; Maziyar, A. et al. Nanoindentational and conventional mechanical properties of spark plasma sintered Ti-Mo alloys. *Journal of materials research and technology* **2020**, *9*, 10647–10658, https://doi.org/10.1016/j.jmrt.2020.07.066.
25. Jixing, L.; Xian, T.; Kun, W. Biodegradable Zn–3Cu and Zn–3Cu–0.2Ti alloys with ultrahigh ductility and antibacterial ability for orthopedic applications. *Journal of Materials Science & Technology* **2021**, *68*, 76–90, https://doi.org/10.1016/j.jmst.2020.06.052.
26. Zhang, D.C.; Mao, Y.F.; Li, YL. Effect of ternary alloying elements on microstructure and superelastictity of Ti–Nb alloys. *Materials Science & Engineering A* **2013**, *559*, 706–710, http://dx.doi.org/10.1016/j.msea.2012.09.012.
27. Abbas, S.N.; Mehdi, S.A.; Seyed, A.D.; Influence of Sintering Temperature on Microstructure and Mechanical Properties of Ti–Mo–B_4C Composites. *Metals and Materials International* **2021**, *27*, 1092–1102, https://doi.org/10.1007/s12540-019-00469-y.
28. Kuroda, P.A.B.; Lourenço, M.L.; Correa, D.R.N. et al. Thermomechanical treatments influence on the phase composition, microstructure, and selected mechanical properties of Ti-20Zr-Mo alloys system for biomedical applications. *Journal of Alloys and Compounds* **2020**, *812*, 1-7, https://doi.org/10.1016/j.jallcom.2019.152108.
29. Pengfei, J.; Bohan, C.; Bo, L. et al. Influence of Nb addition on microstructural evolution and compression mechanical properties of Ti-Zr alloys. *Journal of Materials Science & Technology* **2021**, *69*, 7–14, https://doi.org/10.1016/j.jmst.2020.03.092.
30. Li, FC.; Liu, T.; Zhang, J.Y. et al. Amorphous-nanocrystalline alloys: fabrication, properties, andapplications. *Materials Today Advances* **2019**, *4*, 1-20, https://doi.org/10.1016/j.mtadv.2019.100027.
31. Inoue, A. Amorphous, nanoquasicrystalline and nanocrystalline alloys in Al-based systems. *Progress in Materials Science* **1998**, *43*,365–520, https://doi.org/10.1016/S0079-6425(98)00005-X.
32. Eksi, A.; Kulekci, M.K. Hardness and densification behaviour of copper and bronze powders compacted with uniaxial die and cold isostatic pressing processes. *METABK* **2004,** 43, 129-134. ISSN 0543-5846.
33. German, R. M.: Powder Metallurgy Science, Metal Powder Industries Federation. *New Jersey*, **1994**, 132-146.
34. Chudoba, T.; Schwaller, P.; Rabe, R. et al. Comparison of nanoindentation results obtained with Berkovich and Cube Corner indenters. *Philos. Mag* **1986**, *86*, 5265–5283, https://doi.org/10.1080/14786430600746424.

35. Pradeep, N.B.; Venkatesha, B.K.; Parameshwara, S. et al. Synthesis of nanostructured ternary Ti based alloy for bio-medical applications. *Materials today proceedings* **2021**, https://doi.org/10.1016/j.matpr.2021.09.429.
36. Mrutyunjay, Panigrahi.; Baris, Avar.Development of microstructural and magnetic properties of Co50Si50 alloy powders during mechanical alloying approach. *Applied Physics A* **2021**, *127*, 967, https://doi.org/10.1007/s00339-021-05121-4.
37. Panigrahi, M.; Avar, B. Influence of mechanical alloying on structural, thermal, and magnetic properties of Fe50Ni10Co10Ti10B20 high entropy soft magnetic alloy. *J Mater Sci: Mater Electron* **2021,** *32*, 21124–21134, https://doi.org/10.1007/s10854-021-06612-z.
38. Dekhil, L.; Louidi, S.; Bououdina, M. et al. Microstructural, Magnetic, and Nanoindentation Studies of the Ball-Milled $Ti_{80}Ni_{20}$ Alloy. *Journal of Superconductivity and Novel Magnetism* **2019**, *32*, 3623–3636, https://doi.org/10.1007/s10948-019-05145-1.
39. Pradeep, N.B.; Rajath, H.M.M.; Manjunath, P.G.C.; Khaled, Giasin.; Danil, Yu Pimenov.; Szymon, Wojciechowski. Synthesis and characterization of mechanically alloyed Nanostructured Ternary Titanium Based Alloy for Bio-Medical Applications. *Journal of material research & technology* **2021**, *16*, 88-101, https://doi.org/10.1016/j.jmrt.2021.11.101.
40. Shashanka, R.; Chaira, D. Phase transformation and microstructure study of nanostructured austenitic and ferritic stainless steel powders prepared by planetary milling. *Powder Technol* **2014**, *259*, 125–136, https://doi.org/10.1016/j.powtec.2014.03.061.
41. Shashanka, R.; Chaira, D. Development of nanostructured duplex and ferritic stainless steel by pulverisette planetary milling followed by pressureless sintering. *Mater Charact.* **2015**, *99*, 220-229, https://doi.org/10.1016/j.matchar.2014.11.030.
42. Shashanka, R.; Chaira, D. Optimization of milling parameters for the synthesis of nanostructured duplex and ferritic stainless steel powders by high energy planetary milling. *Powder Technol*ogy **2015,** *278*, 35-45, https://doi.org/10.1016/j.powtec.2015.03.007.
43. Shashanka, R.; Chaira, D. Swamy BEK. Electrocatalytic Response of Duplex and Yittria Dispersed Duplex Stainless Steel Modified Carbon Paste Electrode in Detecting Folic Acid Using Cyclic Voltammetry. *Int. J. Electrochem. Sci*. **2015**, *10*, 5586–5598.
44. Shalabh, G.; Shashanka, R.; Chaira, D. Synthesis of nanostructured duplex and ferritic stainless steel powders by planetary milling: An experimental and simulation study. *IOP Conf. Series: Materials Science and Engineering* **2015**, *75*, 1-7, https://doi.org/10.1088/1757-899X/75/1/012033.
45. Shashanka, R.; Chaira, D. Effects of Nano-Y_2O_3 and Sintering Parameters on the Fabrication of PM Duplex and Ferritic Stainless Steels. *Acta Metall. Sin. (Engl. Lett.)* **2016**, *29*, 58-71, https://doi.org/10.1007/s40195-015-0362-1.
46. Roy, D.; Sinha, A.; Chattopadhyay, P.P. et al. Nanoindentation behavior of bulk metastable Al65Cu20Ti alloy prepared by consolidation of the ballmilled powder. *Materials Science and Engineering A* **2011**, *528*, 8047–8050, https://doi.org/10.1016/j.msea.2011.07.020.
47. Upadrasta, R.; Jae-il, J. Nanoindentation for probing the mechanical behaviour of molecular crystals–a review of the technique and how to use it. *CrystEngComm*. **2014**, *16*, 12-23, https://doi.org/10.1039/C3CE41266K.
48. Yong, L.; Kaiyang, L.; Tao, L. et al. Powder metallurgical low-modulus Ti–Mg alloys for biomedical applications. *Materials Science and Engineering C* **2015**, *56*, 241–250. http://dx.doi.org/10.1016/j.msec.2015.06.010.
49. Lawrence Katz, J. Anisotropy of Young's modulus of bone. *Nature* **1980**, 283, 106-107, https://doi.org/10.1038/283106a0.
50. Wang, X. J.; Chen, X. B.; Hodgson, P. D.; Wen, C. E. Elastic modulus and hardness of cortical and trabecular bovine bone measured by nanoindentation. *Trans. Nonferrous Met. SOCChina* **2006,**16,744-748, https://doi.org/10.1016/S1003-6326(06)60293-8.
51. Edward Hoffler, C.; Edward Guo, X.;Philippe K. Z.; Steven A. G. An Application of Nanoindentation Technique to Measure Bone Tissue Lamellae Properties. *Journal of Biomechanical Engineering* **2006**, 127, 1046-1053.
52. Geetha, M.; Singh, A.K.; Asokamani, R. et al. Ti based biomaterials, the ultimate choice for orthopaedic implants – A review. *Progress in Materials Science* **2009**, *54*, 397–425, https://doi.org/10.1016/j.pmatsci.2008.06.004.

53. Zhang, L.C.; Liu, Y. Additive manufacturing of titanium alloys for biomedical applications. In: Addit. Manuf. Emerg. *Mater.Springer International Publishing. Cham* **2019**, 179–196, http://dx.doi.org/10.1007/978-3-319-91713-9-5.
54. Baltatu, M.S.; Vizureanu, P.; Tierean, M.H. et al. Ti-Mo alloys used in medical applications. *Adv. Mater. Res.* **2015**, *1128*, 105–111, https://doi.org/10.4028/www.scientific.net/AMR.1128.105.